Nonlinear Creep in a Polymer Glass

Robert A. Riggleman,[†] Kenneth S. Schweizer,[‡] and Juan J. de Pablo*,[†]

Department of Chemical and Biological Engineering, University of Wisconsin, Madison, Wisconsin, 53706, and Departments of Materials Science and Chemistry, University of Illinois, Urbana, Illinois, 61801

Received January 17, 2008; In Final Form May 5, 2008; Revised Manuscript Received April 22, 2008

ABSTRACT: Results of molecular dynamics simulations are presented for the nonlinear creep response of a model polymer glass under both tension and compression. The structure of the material was examined as a function of time; it is found that the overall structure, as measured by the structure factor, changes appreciably during the deformation. The intensity of the first peak is decreased under stress and the polymer chains are deformed. The dynamics are studied using both the bond autocorrelation function and the incoherent dynamic structure factor. It is found that the dynamics are strongly correlated with the strain rate in the material. Additionally, each measure of the dynamics is uniformly enhanced by the same amount. Previous simulations have shown that the enhanced dynamics do not correlate with changes in the volume in any clear manner; here, evidence from simulations indicates that the enhanced dynamics correlate with the energy of the inherent structures of the material, suggesting that changes in the materials' position on the potential energy landscape lead to the observed enhanced dynamics. Finally, the results of simulations are discussed in terms of two theories of stress-induced dynamics.

1. Introduction

The influence of deformation on the mobility of polymeric and molecular glasses has received considerable attention. The experiments of Loo and co-workers served to establish that the number of mobile bonds increases in the amorphous domains of semicrystalline Nylon-6 during deformation at the glass transition temperature, T_g.[1] Experiments by Zhou and co-workers also showed that the uptake of diluents by glassy polymers under deformation 100 °C below T_g is comparable to that of the undeformed polymers at T_g.[2,3] More recently, Lee and Ediger have employed fluorescence recovery after photobleaching to measure the dynamics of lightly cross-linked poly(methyl methacrylate) samples undergoing creep just below the glass transition temperature;[4] they find that the relaxation times are decreased significantly compared to the relaxation times in the material at rest. Decreases of over 2 orders of magnitude are observed for several of their experiments. While there is strong experimental evidence supporting enhanced dynamics during deformation, the origin of such dynamics remains elusive.

Several simulation studies have examined the effects of deformation on the properties and dynamics of amorphous materials; the most widely studied system to date has been the binary Lennard-Jones (LJ) glass model. Lacks and co-workers investigated how shear deformations can alter the inherent structure energy of the binary LJ glass and found that deformation can lead to the destruction of energy barriers between inherent structures on the potential energy landscape (PEL).[5–7] These authors also offered an explanation for "overaging" and "rejuvenation" in amorphous materials in terms of their PEL analysis.[5] Additionally, Berthier and Barrat showed that the viscosity of the binary LJ glass exhibits strong shear-thinning behavior in the glassy state when deformed at high shear rates.[8] Varnik arrived at similar conclusions.[9] Nandagopal and Utz compared thermal motion to deformation-induced motion and reported that the deformation-induced motion occurs independently and alongside thermal motion.[10,11]

Simulation studies of deformation-induced dynamics in polymeric systems have been scarce. Capaldi and co-workers investigated how strain modifies the gauche–trans transition

rate in glassy polyethylene during compression at a constant strain rate. They observed an increased transition rate during the deformation, which decreased after the deformation was stopped; no correlation between the dynamics and the free volume was detected in their studies.[12,13] Lyulin and co-workers investigated the dynamics in fully atomistic polycarbonate and polystyrene during active deformation;[14,15] they reported that the dynamics were minimally enhanced below the yield strain and then became increasingly faster than the undeformed sample beyond the yield point. Warren and Rottler performed simulations of a polymer glass under tensile stress to study the effects of aging on the creep compliance and the deformation-induced mobility.[16] They showed that the dynamics and mechanical shift factors each change by the same relative amount with aging time and applied stress.

More recently, we have studied the nonlinear creep response of a coarse grain polymer glass[17] and arrived at two central results. First, it was shown that there are appreciable finite-size effects for systems with box sizes (L) smaller than $L \approx 2\xi$, where ξ is the length scale associated with mechanical heterogeneity.[18–20] Second, the dynamics were shown to correlate strongly with strain rate, regardless of whether the material was subject to tensile or compressive stresses. Consistent with the results of Capaldi et al.,[12] no correlation was observed between the dynamics and the changes in volume in the system during compression simulations.

One question that remains unanswered, however, is whether a common physical property can be identified in both compressive and tensile deformations to explain the enhanced dynamics. In this study, we extend the results of our previous work[17] by studying changes in the structure of our polymer glass and by studying other measures of the dynamics in our system. We find that both the overall structure of the system (as measured by the structure factor, $S(q)$), is affected by the deformation and that the individual polymer chains are drastically deformed. Additionally, the deformation of the polymer chains changes as the deformation proceeds. The chain deformation is purely affine (i.e., the same as the deformation of the simulation box) for small strains and becomes smaller than the affine deformation for larger strains. By using the dynamic incoherent structure factor to study the dynamics, $F_s(q, t)$ at two different values of q, we examine how the dynamics are enhanced on various length scales. For the values of q investigated here, we find that the

* Corresponding author. E-mail: depablo@engr.wisc.edu.
† University of Wisconsin.
‡ University of Illinois.

dynamics are universally enhanced by approximately the same amount. The amount of enhancement appears to correlate strongly with the "instantaneous" strain rate that the material experiences at a given point in time, as shown previously,[17] as well as with changes in the inherent structure energy. The dynamics in both tension and compression appear to correlate in a uniform manner with the changes in the inherent structure energy, indicating that the PEL provides an appropriate framework to understand deformation-induced dynamics. Finally, we compare our results to the predictions of both the Eyring model[21] and the recent model of Chen and Schweizer for stress-induced dynamics.[22]

2. Methods

The equilibrium properties and glass transition behavior of the model considered here have been characterized extensively in previous works,[23–26] and we only recount some of the details of the model here for completeness. Our polymer chains consist of 32 Lennard-Jones (LJ) sites connected by stiff harmonic springs. The LJ potential in our system is shifted such that it goes smoothly to zero at the cutoff distance, which was set to be $r_{cut} = 2.5$. All units in this paper are in LJ units of the polymer monomer (i.e., $T/T^* = R/\varepsilon_A$; $P/P^* = \sigma_A^3/\varepsilon_A$; $t/t^* = \sqrt{\theta_A^2 m/\varepsilon_A}$, where the asterisk implies real units, R is the gas constant, and ε_A and σ_A are the LJ parameters for the polymer monomers). Our time step, δt, was taken to be $\delta t = 0.001$.

Five independent configurations were generated at a high temperature using a combination of Monte Carlo (including double-bridging moves) and molecular dynamics techniques. The systems were then cooled from $T = 1.0$ to the $T = 0.37$ in the NPT ensemble at zero pressure. The glass transition temperature, T_g, for this system has been previously reported to be in the range $0.37 \leq T_g \leq 0.40$, depending on the technique employed to estimate T_g;[25,27] the procedure employed here, therefore, cools our system into the glassy regime, where we still expect to observe a viscous response to an applied stress on a reasonable time scale. After cooling to $T = 0.37$, the ensemble was switched from the NPT ensemble to NσT,[28] where σ represents the full stress tensor. The use of the NσT ensemble enables our simulation box to adopt any parallelepiped shape and relax stresses in any direction, including shear stresses. Next, our configurations were aged for 2×10^6 time steps using molecular dynamics before a constant stress was applied in the z direction, σ_{zz}, and the systems were allowed to deform using molecular dynamics. Both tensile and compressive stresses were employed, and the response of the system as a function of time was measured. All other components of the stress tensor remained set to zero, and all deformation simulations were performed using the Gromacs simulation package.[29,30] Before applying the stress, the average density of the systems was found to be $\rho = 1.02$. In this work, we consider two different system sizes: one containing 176 polymer chains and a second containing 1244 chains. At this density, these sizes correspond to boxes where the primary axes have initial lengths $L_0 = 17.7$ and 33.9, respectively; both of these values of L_0 are greater than twice the correlation length for mechanical heterogeneity,[18] ξ. For the model considered here, ξ has been previously shown to be $\xi = 8$.[31] Our previous work has also demonstrated that systems of this size do not exhibit significant finite-size effects during the types of deformations presented here.[17]

3. Results

3.1. Changes in Structure. First, we report the creep compliance of our system for the various applied stresses. The creep compliance, denoted by $J(t)$, is defined as $J(t) = \varepsilon(t)/\sigma_{zz}$, where $\varepsilon(t)$ is the time-dependent strain. We define the strain as $\varepsilon(t) = L_z(t)/L_0 - 1$, where $L_z(t)$ is the instantaneous length of
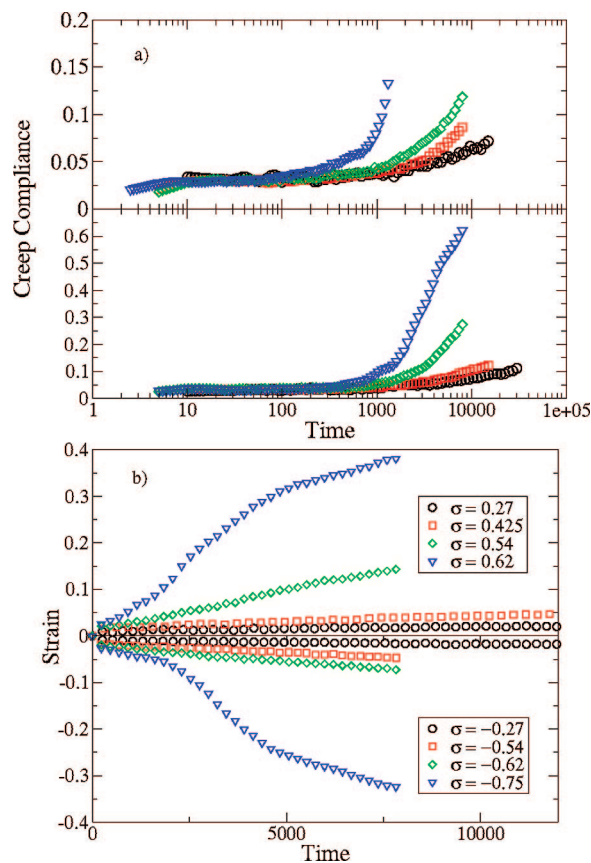

Figure 1. (a) Creep compliance for systems under compression (top) under a stress of $\sigma_{zz} = -0.27(\bigcirc)$, $-0.54(\square)$, $-0.62(\diamondsuit)$, and $-0.75(\triangledown)$. The bottom four curves show the creep compliance for systems under tension with $\sigma_{zz} = 0.27(\bigcirc)$, $0.425(\square)$, $0.54(\diamondsuit)$, and $0.62(\triangledown)$. (b) Strain as a function of time for all applied stresses. All curves are averaged over five configurations of size $L_0 = 17.7$.

the box in the z direction. Figure 1a shows $J(t)$ for all values of applied stress; it is clear that we are well into the nonlinear creep regime[32] for both the tensile and compressive stresses. The smallest stresses approach the linear regime. For comparison, when we perform tensile deformations of our polymer at a constant strain rate of 10^{-4}, the yield stress is approximately $\sigma = 0.61$. Figure 1b shows the strain as a function of time for each deformation. As the applied stress increases, both the strain and strain rate increase, as expected. Interestingly, in most cases there is an extended linear dependence of the strain on time. Naively, this could be interpreted as viscous flow; this is not likely to be a fully developed viscous flow, due to the relatively short time scales sampled by our simulations. However, this constant strain rate regime may be indicative of a viscous flow-like process on the segmental length and time scales probed by our simulations.

Since our use of the NσT ensemble allows the shape (and therefore the volume) of our simulation box to fluctuate as the simulation proceeds, it is of interest to examine how the volume changes during each deformation. Figure 2 shows the relative volume as a function of time for all values of applied stress. For systems under tensile stress, the volume increases monotonically with increasing applied stress. The volume increases immediately after applying the tensile stress and remains constant for all but the largest stress, in which case volume goes through a maximum and then decreases as the simulation proceeds. For compressive stresses, the situation is less clear. There is a decrease in the volume immediately after the stress is applied; however, the amount of the decrease does not clearly correlate with the applied stress. The smallest decrease is found
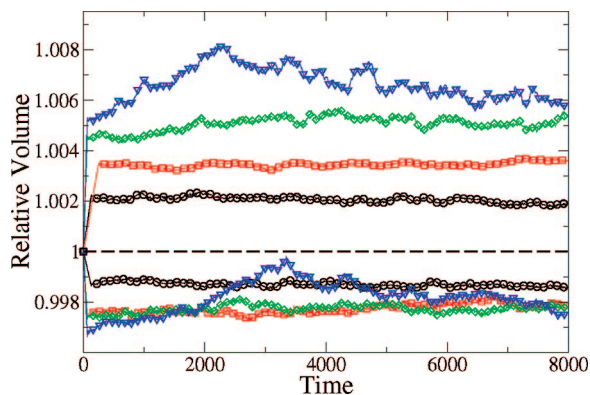
Figure 2. Relative volume as a function of time averaged over all configurations of size $L = 17.7$ for systems under compression (below the dashed line) under a stress of $\sigma_{zz} = -0.27(\bigcirc)$, $-0.54(\square)$, $-0.62(\diamondsuit)$, and $-0.75(\nabla)$. Above the horizontal, dashed line are the results for systems under tension with $\sigma_{zz} = 0.27(\bigcirc)$, $0.425(\square)$, $0.54(\diamondsuit)$, and $0.62(\nabla)$.
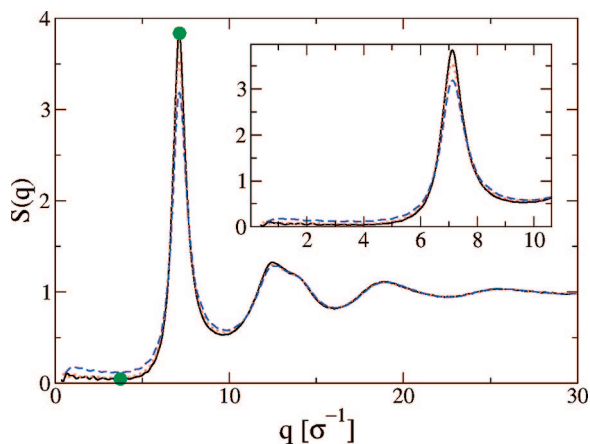

Figure 3. Structure factor for the unstressed system (solid line), the system under tension with $\sigma_{zz} = 0.62$ (dotted line), and the system under compression with $\sigma_{zz} = -0.75$ (dashed line). The inset is a closer view of the low-q part of the structure factor. The filled circles indicate the q values used to calculate $F_s(q, t)$.

for the smallest applied stress ($\sigma_{zz} = -0.27$), but for stresses of $\sigma_{zz} = -0.54$ and -0.62, the decrease is comparable. For an applied stress of $\sigma_{zz} = -0.75$, the volume change is not constant with time, similar to the volume behavior observed for the largest applied tensile stress.

Having established that the volume changes slightly during our deformations, we turn our attention to changes in the overall structure of our material as measured by the static structure factor, $S(q)$. Since we expect any changes in the structure to be most prevalent for the largest applied stresses, we only report $S(q)$ averaged over the final configurations after experiencing the largest tensile and compressive stresses, $\sigma_{zz} = -0.75$ and 0.62, respectively. These results are shown in Figure 3 and $S(q)$ from the undeformed samples is also shown for comparison. The intensity of the first peak of $S(q)$ is decreased (see inset to Figure 3) for both stresses, indicating a reduction in order in the system. For values of $q \geq 12$, each $S(q)$ curve is essentially indistinguishable. For the systems deformed with compressive stress $\sigma_{zz} = -0.75$, the intensity of $S(q)$ in the low-q regime ($q \leq 6$) is higher than both the undeformed sample and the sample deformed with a tensile stress $\sigma_{zz} = 0.62$. This indicates that stress reduces local cage order and enhances the amplitude of long wavelength density fluctuations (i.e., $q \leq 6$) corresponding to deformation-induced structural disordering.

In addition to changes of the structure as measured by $S(q)$, we can examine to what extent the individual polymer chains
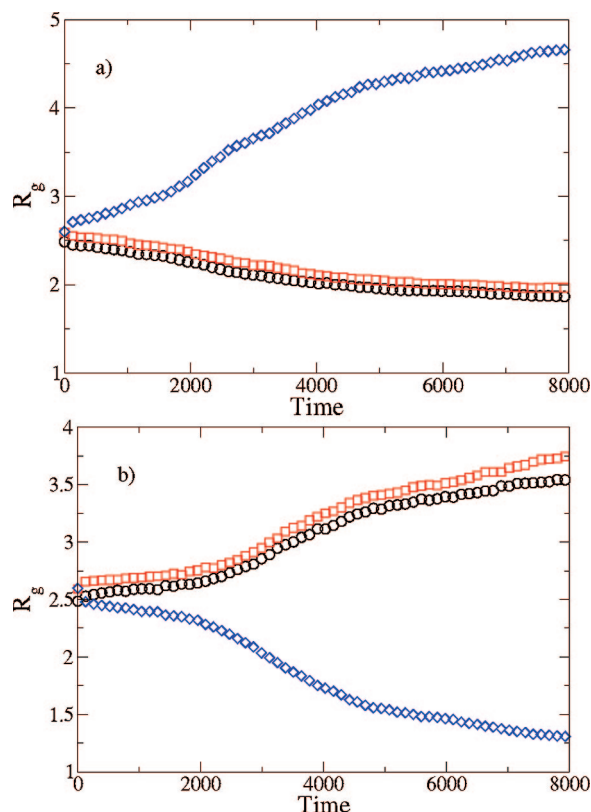

Figure 4. Evolution of the components of the radius of gyration, $R_{g,x}$ ($\bigcirc$), $R_{g,y}$ ($\square$), and $R_{g,z}$ ($\diamondsuit$) with time for the systems under stress with $\sigma_{zz} = 0.62$ (a) and $\sigma_{zz} = -0.75$ (b).

are deformed by examining the structure of the chains. To that end, we calculate the three components of the radius of gyration, denoted by $R_{g,x}(t)$, $R_{g,y}(t)$, and $R_{g,z}(t)$ (Figure 4). For both cases, we find that the component of R_g in the direction of deformation, the z direction, changes in the same manner as the simulation box. During tension, the x and y components of R_g contract as the chains become elongated in the direction of applied stress. In compression, we find the opposite trend; as the chains are compressed in the z direction, they expand in the x and y directions.

It is of interest to compare the relative changes of R_g to the overall deformations of the simulation box in order to examine whether or not the chain deformations are purely affine. Figure 5 shows the instantaneous relative value of $R_{g,z}(t)$ plotted against the instantaneous strain at several time points during our deformation simulations for two values of tensile (Figure 5a,b) and compressive (Figure 5c,d) stresses. If the chains are deformed in an affine manner (i.e., the deformation of the chains is the same as that of the simulation box), one would expect these points to lie along the line $y = x + 1$. For the smaller values of stress shown ($\sigma_{zz} = 0.425$ and -0.54 shown in panels a and c of Figure 5, respectively), this is the behavior we observe; each of the points lies close to the line $y = x + 1$. However, for the largest values of stress ($\sigma_{zz} = 0.62$ and -0.75 shown in panels b and d of Figure 5, respectively), this is only the case for small strains. Once the system has been strained beyond $\varepsilon \approx 0.12$, the deformation of the chains deviates from the affine deformation and generally experiences a smaller deformation than the overall system. Interestingly, for these two larger values of applied stress, this value of strain is approximately the strain where the strain rate increases (see Figure 1b).

Using the three components of R_g, we can define an effective chain volume, denoted by $V_{ch}(t)$, as

$$V_{ch}(t) = R_{g,x}(t) \cdot R_{g,y}(t) \cdot R_{g,z}(t) \qquad (1)$$

where $R_{g,x}(t)$ and $R_{g,y}(t)$ are the x and y components of the radius of gyration, similar to $R_{g,z}(t)$ above. Figure 6 shows the relative chain volume ($V_{ch}(t)/V_{ch}(0)$) during the deformations with $\sigma = 0.62$ and -0.75. For the systems under tension, we find that the relative chain volume increases immediately after the
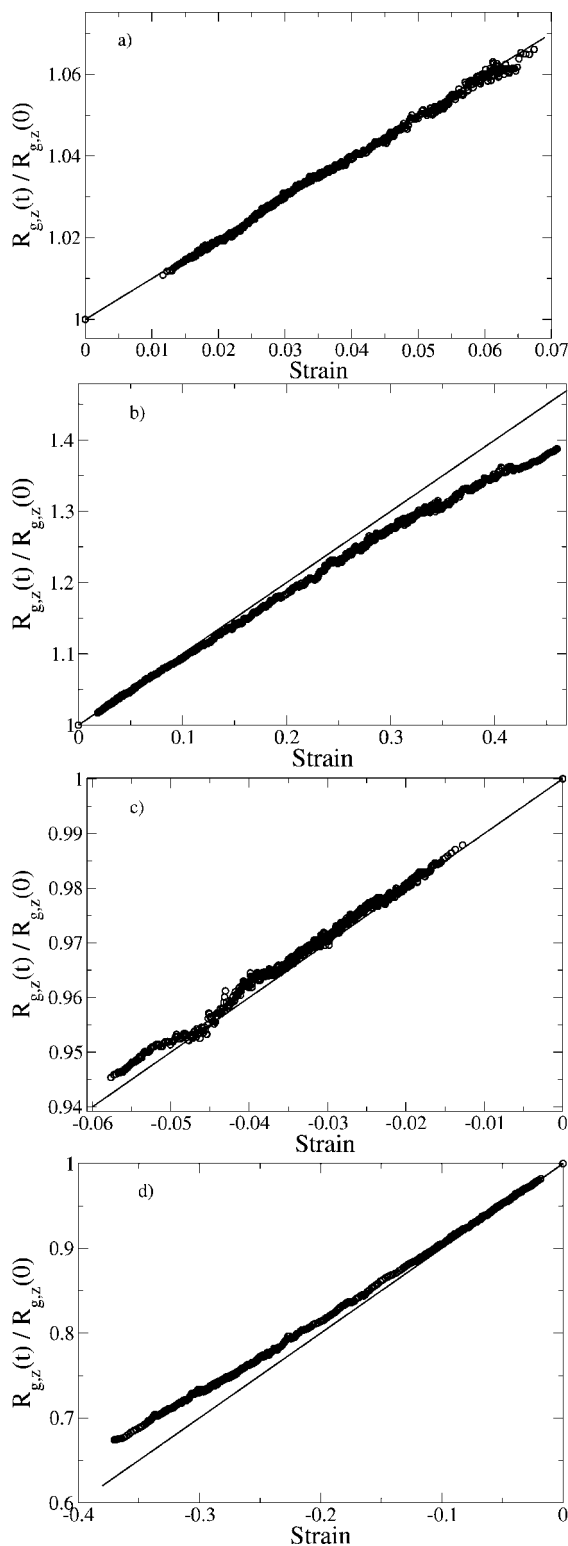

Figure 6. Relative volume of the polymer chains during deformation with $\sigma = 0.62$ (○) and $\sigma = -0.75$ (□). For comparison, the relative volume of the system during the deformation with $\sigma = 0.62$ (dashed line) and $\sigma = -0.75$ (dot-dashed line).

Figure 7. Strain response for individual configurations under tension with $\sigma_{zz} = 0.54$. The symbols (□), (○), (◇), (left pointing triangle), and (△) are from configurations with $L_0 = 17.7$, while the (+), (×), and (∗) symbols are from configurations with $L_0 = 33.9$.

application of the stress, similar to the overall system volume. In compression, however, the response is different. Initially, the chain volume decreases similar to the system volume; presumably this is a result of an affine deformation of the chains. For times greater than 500, however, the effective chain volume increases, even beyond the values observed for the systems under tension. Changes in coil volume will modify the number of interpenetrating chains and hence intermolecular contacts.

3.2. Dynamics During Deformation. We now turn our attention to the dynamics of the polymer glass under stress. We find it useful to measure the dynamics of individual configurations, and we begin by plotting the strain response for each configuration with $\sigma_{zz} = 0.54$ in Figure 7. While there is some variability in the strain response of our glass, if we average over all configurations, the response is essentially identical for the systems with $L_0 = 17.7$ and 33.9, as we have shown previously.[17] Because the dynamics are so sensitive to the instantaneous properties of the material (e.g., the strain rate), we find it beneficial to not average over independent configurations; none of the conclusions discussed below are sensitive to this approach. Since we wish to measure the dynamics as our systems deform and we have already demonstrated that various properties such as the strain rate (Figure 1) are not constant with time, it is useful for us to define time windows during which we measure the dynamics so that we are able to compare the changes in the dynamics to the changes in other properties of the system. We note that none of the conclusions discussed below are sensitive to our choice of time windows. For $\sigma_{zz} = 0.54$, these windows are indicated in Figure 7. To measure the

Figure 5. Instantaneous relative changes in the z component of the radius of gyration plotted against the instantaneous strain for systems with applied stresses (a) $\sigma_{zz} = 0.425$, (b) $\sigma_{zz} = 0.62$, (c) $\sigma_{zz} = -0.54$, and (d) $\sigma_{zz} = -0.75$. In all four figures the solid line represents $y = x + 1$. Results are averaged over all configurations for each stress.
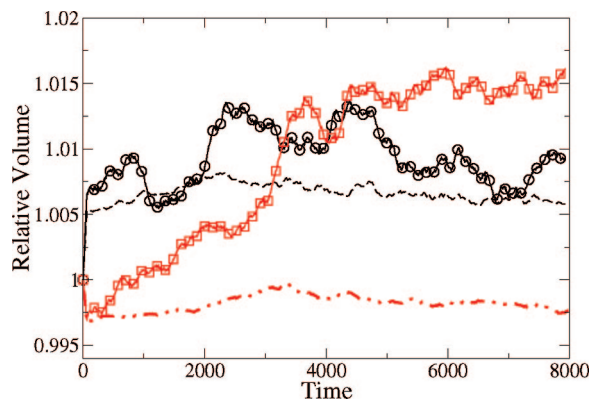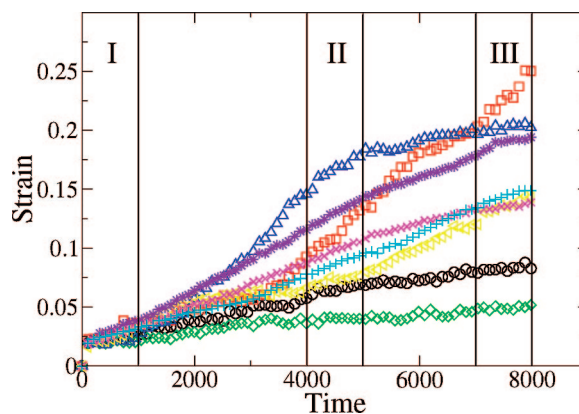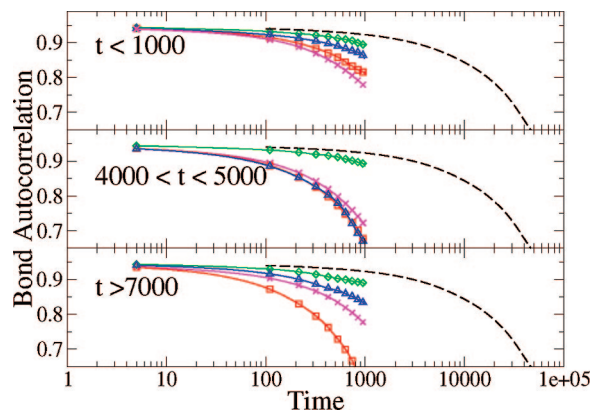
Figure 8. $C_b(t)$ for sample configurations during various time windows. The time on the x axis refers to the elapsed time since the beginning of the time window, and the text labels define the range of time of the full deformation trajectory during which $C_b(t)$ was determined. The time windows are also denoted in Figure 7. The dashed black line represents the average $C_b(t)$ for the unstrained samples. The symbols represent the same configurations as in Figure 7.

Figure 9. Relaxation time plotted against the absolute value of the strain rate during various time windows. The strain rates are averaged over their values during each time window. The symbols represent systems under tension with $\sigma_{zz} = 0.62$ ($\Box$), 0.52 ($\bigcirc$), 0.425 ($*$), and 0.27 ($\Diamond$) and under compression with $\sigma_{zz}=0.75$ (right pointing triangle), 0.62 (left pointing triangle), 0.54 ($\triangle$), and 0.27 (∇). The dashed horizontal line indicates the value of the relaxation time from the undeformed sample. The solid line shows $\tau \propto \dot{\varepsilon}^{-1}$. Open symbols are from configurations with $L = 17.7$ and filled symbols with $L = 33.9$.

dynamics, we employ the bond autocorrelation function, denoted by $C_b(t)$, which is defined as $C_b(t) = \langle P_2[\hat{b}(t)\cdot\hat{b}(0)]\rangle$, where P_2 is the second Legendre polynomial and $\hat{b}(t)$ is a unit vector aligned along the bonds of the polymer chain. This function has been used previously in many studies of the dynamics of amorphous polymers.[24,25,33] In order to prevent any trivial contribution to the dynamics, we have removed the affine displacements (those resulting from the deformation of the simulation box) from the total particle displacements before calculating $C_b(t)$. Figure 8 plots $C_b(t)$ for four configurations during the time windows indicated in Figure 7. Also included in Figure 8 is $C_b(t)$ taken from an extremely long molecular dynamics run on an undeformed sample at the same temperature; these calculations to obtain the undeformed response were begun after the aging step in our material's thermal history. The dynamics of the deformed samples are clearly enhanced for all configurations relative to the undeformed response. Another point to note is that for a given applied stress, the dynamics are not constant. As shown previously,[17] we find that the dynamics are enhanced the most during times of high strain rate. For example, the configuration indicated by triangles deforms slowly (i.e., low strain rate) after application of the stress. In the second time window, the strain rate is higher, and in the final time window, it decreases again (see Figure 7). The behaviors of $C_b(t)$ follow a similar trend; during the second time window it decays much faster than the first and last time windows.

We wish to develop a technique that will allow us to more quantitatively measure the extent to which the dynamics are enhanced. As we have done previously,[17] we fit the dynamic property of interest ($C_b(t)$ or $F_s(q, t)$, described below) from the unstressed molecular dynamics runs to a Kohlrausch–Williams–Watts (KWW) equation of the form

$$C(t) = C_0\exp\left[-\left(\frac{t}{\tau}\right)^{\beta}\right], \qquad (2)$$

where $C(t)$ is either $C_b(t)$ or $F_s(q, t)$, C_0 is a pre-exponential factor, β is the stretching exponent, and we use τ as a measure of the dynamics. Next, we fit the dynamic response in the systems undergoing deformation to eq 2 while keeping β fixed at its value from the undeformed sample. We choose to keep β fixed for simplicity, and we note that none of the conclusions discussed below change in any way if β is allowed to change. This enables us to obtain τ for the deforming sample. We note that eq 2 assumes a single relaxation process is dominant over the probed time scales and possible complications due to
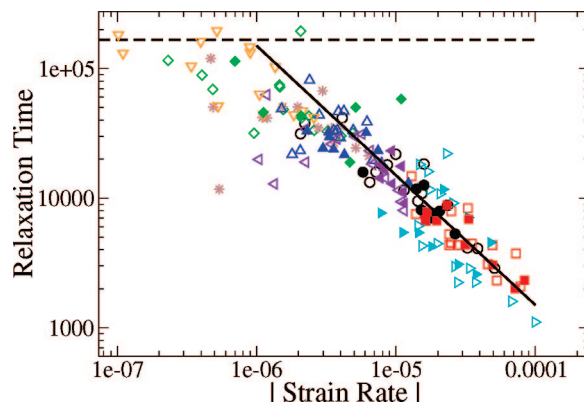
overlapping fast (e.g., β-relaxation) and slow (e.g., α-relaxation) relaxations are not addressed. Hence, we do not consider τ to be a measure of the structural relaxation time in our samples but merely a measure of the change in dynamics during the time windows of our deformation simulations.

Figure 9 is a plot of τ obtained from $C_b(t)$ plotted against the absolute value of the strain rate for the time windows during deformation. The strain rates are obtained for each time window by numerically differentiating the strain versus time plots using a central difference method and averaging over the time window. There is a clear correlation of the enhanced dynamics with the absolute value of the strain rate ($\dot{\varepsilon}$) during each time window. Remarkably, the estimates of τ as obtained from either compression or tension each lie on the same curve and apparently have the same dependence on $\dot{\varepsilon}$ within the scatter of our data. Here, we again point out that we have not averaged the results for τ over our independent configurations, and this contributes to the scatter in our results. For strain rates above $\dot{\varepsilon} \approx 3 \times 10^{-6}$, we find that $\tau \propto \dot{\varepsilon}^{-1}$. Overall, the data presented in Figure 9a are reminiscent of the viscosity data in a shear-thinning fluid, although the scatter in the data in Figure 9 implies that there are likely other causes (such as the applied stress, discussed below) for the enhanced dynamics than only the strain rate. Similar correlations in the dynamics of a polymer glass undergoing shear at a constant strain rate have been observed previously for the binary Lennard-Jones glass.[8,9] Here we wish to again emphasize that the strain rate is not the controlled variable in our calculations, and due to the complex viscoelastic response of our polymer glass, the strain rate changes with time.

Given that the results shown above and our previous work[17] have demonstrated that the dynamics as measured by $C_b(t)$ correlate very strongly with the strain rate, it is of interest to examine other measures of the dynamics and determine if and to what extent they are affected by the applied stress. To that end, we calculate $F_s(q, t)$, the dynamic incoherent structure factor, where

$$F_s(q, t) = \langle\cos(\vec{q}\cdot[\vec{r}_i(t) - \vec{r}_i(0)])\rangle \qquad (3)$$

Here, q is the chosen wavevector and $r_i(t)$ is the position of particle i at time t. Figure 10a shows a comparison of $F_s(q, t)$ for two values of q with $C_b(t)$. The values of q were chosen to be the q associated with the maximum of the first peak in $S(q)$ ($q = 7.14$) and a smaller value in the flat region of $S(q)$ ($q =$
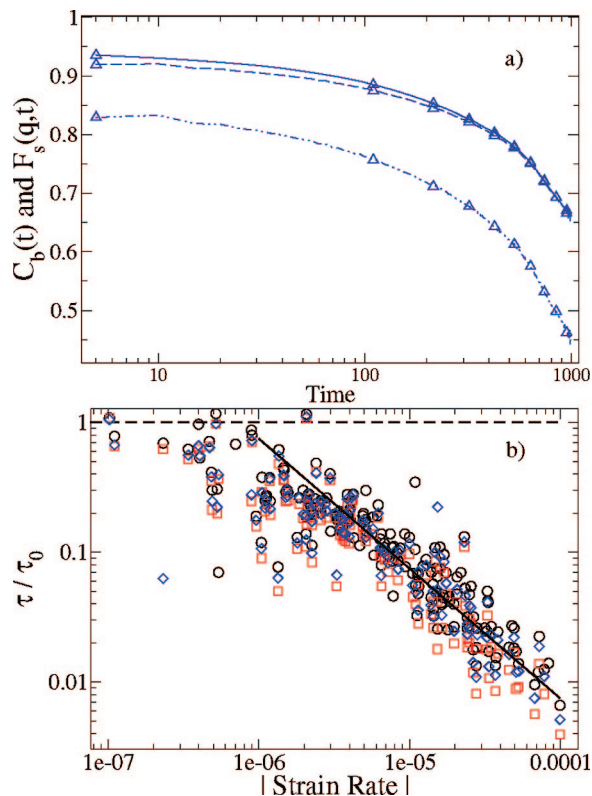
Figure 10. (a) Comparison of $F_s(q, t)$ for two different values of q and $C_b(t)$ for the same configuration and time window. $C_b(t)$ is shown in solid lines, $F_s(q = 3.74, t)$ is shown with a dashed line, and $F_s(q = 7.14, t)$ is plotted with the dash-dot line. (b) Relaxation time obtained from $C_b(t)$ ($\bigcirc$), $F_s(q = 7.14, t)$ ($\square$), and $F_s(q = 3.74, t)$ ($\diamond$) normalized by τ from the undeformed samples, denoted by τ_0. The dashed horizontal line corresponds to $\tau/\tau_0 = 1$, and the solid line is $\tau \propto \dot{\varepsilon}^{-1}$.

3.74). These values are indicated in Figure 3 above. From Figure 10a, we see that we do not sample the initial drop of $F_s(q, t)$ from unity to the plateau value. As discussed above, this implies that we are sampling the dynamics that correspond to the end of the β relaxation and the early α relaxation when we fit our results to eq 2. Figure 10b is a plot similar in nature to Figure 9; however, here τ is obtained from fitting the decay of $F_s(q, t)$. The data in Figure 10b are normalized by τ_0, the estimate of τ obtained from eq 2 for the undeformed sample. We find that the relaxation times, τ, obtained using any of these three methods appear to all collapse onto a single curve within the scatter of our data and the dynamics appear to be uniformly enhanced by the applied stresses in our material. For a given strain rate, τ measured from the rotational dynamics of the polymer bonds and τ measured from $F_s(q, t)$ for either value of q are decreased by approximately the same amount, and the approximate scaling $\tau \propto \dot{\varepsilon}^{-1}$ still holds for larger values of $\dot{\varepsilon}$.

Since the dynamics are enhanced by the same amount for $F_s(q, t)$ at two different magnitudes of q, it is of interest to examine whether the dynamics are isotropic. To that end, we repeat the above fitting procedures for $F_s(q, t)$ with q vectors that are in the x, y, or z directions only. This provides a test of whether the dynamics are more enhanced in the direction of applied stress (z direction) or not. Figure 11 plots τ_x and τ_y respectively against τ_z; we find that all of the points lie along the line $y = x$, indicating that the dynamics are enhanced isotropically. The results in ref 10 exhibit a similar behavior under both shear and uniaxial deformations. Hence, despite the large anisotropy of the chain conformations and interchain packing correlations, the deformation results in a remarkably large isotropic acceleration of relaxation.
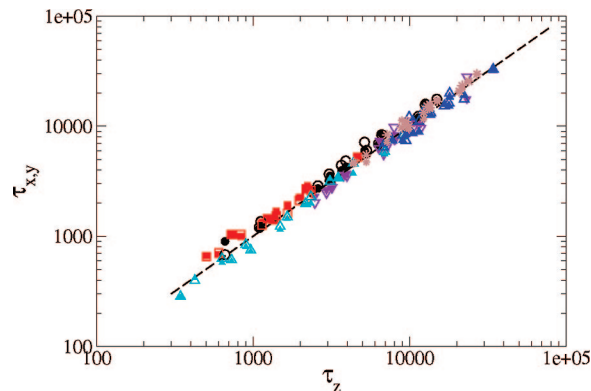

Figure 11. Relaxation time obtained from $F_s(q = 7.0, t)$ in the x-direction (open symbols) and y direction (solid symbols) plotted against $F_s(q = 7.0, t)$ in the z direction for various values of stress.

Given that our previous work has shown that volume changes cannot explain the observed changes in dynamics in our polymer glass,[17] we now propose an alternative explanation of the changes in dynamics. Previous works have demonstrated how applied strain can change the "position" of a material on its PEL.[5–7] As the strain is increased, it has been shown that the potential energy of the material is also increased. We therefore turn to the inherent structure energy, U_{is}, of our polymer glasses. For each of our trajectories, we sample several configurations and minimize the energy of the system using the steepest descent algorithm; i.e., we quench the system into its inherent structure.[34,35] The minimization was stopped when the maximum force was smaller than 10^{-7}, and the minimizations were performed while keeping the box dimensions constant. After minimizing several configurations along our trajectory, we can then observe how the energy of the inherent structures changes as the deformation proceeds and test whether there is any correlation with the dynamics. Figure 12a shows a plot of the change in the inherent structure energy as the deformation proceeds for three configurations under tension with $\sigma_{zz}=0.54$. Once again, we find that the most pronounced effects are observed for configurations currently experiencing a high strain rate. During periods of high strain rate, the configurations move to locations on the PEL that have a higher inherent structure energy. This behavior is qualitatively similar to thermally induced motion in amorphous materials. As the temperature of a glassy system is increased above T_g and into the supercooled liquid regime, the inherent structure potential energy increases.[36] The landscape picture presented in ref 36 is discussed at constant volume, whereas the shape and volume of our simulation box changes with deformation complicating a direct comparison to the changes in E_{is} observed by raising the temperature. As the strain rate is increased, the average value of the inherent structure energy also increases. See the configuration denoted by ($\diamond$) in Figure 12a for an example of this behavior, where the highest inherent structure energies are found during times of highest strain rate (i.e., $2000 < t < 4000$). The behavior of the inherent structure energy with strain rate observed here is consistent with previous studies of the deformation of the binary LJ glass[6] at constant strain rate, although it has also been shown that the inherent structure energy changes with strain before the yield point for deformations at a constant strain rate.[5,37] To further explore the correlation between changes in the inherent structure energy and the dynamics, we have calculated the average change in the inherent structure energies in each time window used to calculate the strain rates and relaxation times above. In Figure 12b, we plot the change in the inherent structure energy against the strain rate for each time window and all applied stresses. For relatively small strain rates ($\dot{\varepsilon} \leq 10^{-5}$), $E_{is}(t)$ increases slowly with strain rate, while during periods of larger strain
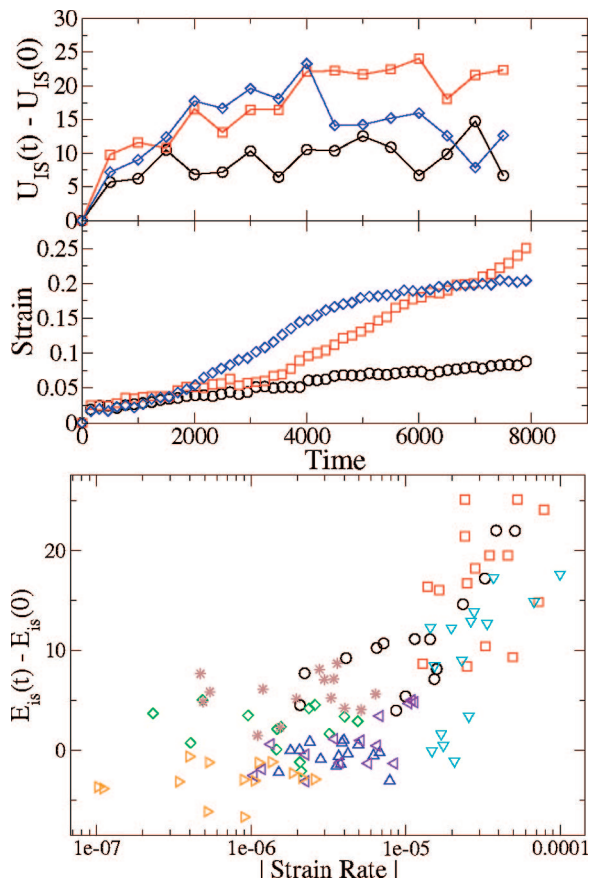
Figure 12. (a) Top: changes in the inherent structure energy as a function of time for three sample configurations. Bottom: strain as a function of time for the same configurations, taken from Figure 7. (b) The changes in the inherent structure measured in each time window plotted against the strain rate. The symbols are the same as those in Figure 9.
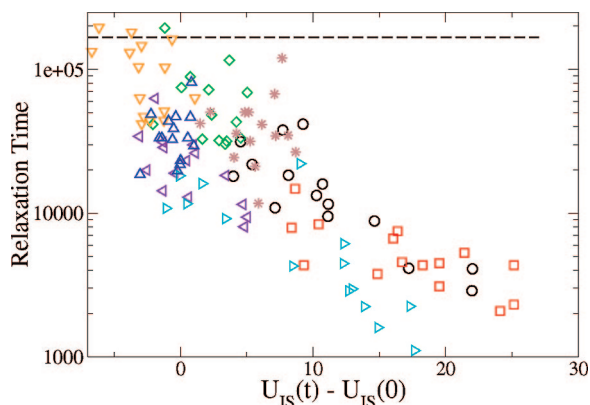

Figure 13. Relaxation time plotted against changes in the inherent structure energy. The symbols represent systems under tension with $\sigma_{zz} = 0.62$ (□), 0.52 (○), 0.425 (∗), and 0.27 (◇) and under compression with $\sigma_{zz} = 0.75$ (right pointing triangle), 0.62 (left pointing triangle), 0.54 (△), and 0.27 (▽).

rates ($\dot{\varepsilon} \geq 10^{-5}$), $E_{is}(t)$ increases much more sharply with strain rate.

Figure 13 shows the correlation between the estimated relaxation times, τ, and the changes in the inherent structure energy. Once again, we calculate each property during the time windows described above. We see from Figure 13 that the material clearly exhibits enhanced mobility when it has a higher inherent structure energy, similar to thermally activated motion. We should point out that previous works have examined the
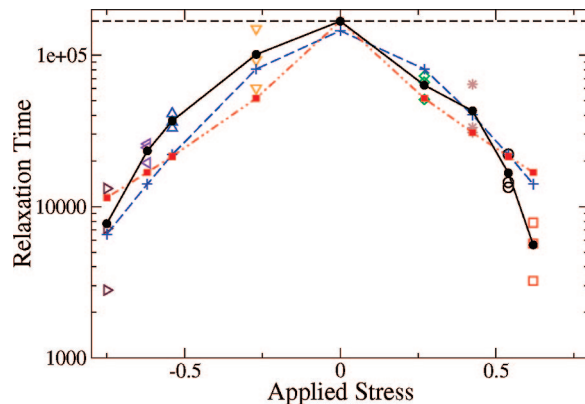

Figure 14. Relaxation times (τ) estimated from $C_b(t)$ for each applied stress, where τ has been averaged over the five $L_0 = 17.7$ configurations. The three points at each stress result from measuring the dynamics at various times during deformation (i.e., different time windows). The solid black circles denote τ if we average over both configurations and time windows, and the solid line is a guide to the eye. The dashed line with the (+) points are results from fitting to eq 6, and the dot-dashed line with the filled square points are the predictions of eq 8.

relationship between thermal motion and deformation-induced motion (at constant strain rate), and it was shown that these processes occur independently of each other to a first approximation.[10] Additionally, the changes in both the shape and volume of our simulation box is expected to deform the underlying energy landscape, rendering a direct comparison of thermal changes in E_{is} to deformation-induced changes difficult. The different changes in volume that we observe (increases during tension and decreases during compression) likely also contribute to the noise in the data shown in Figure 13.

3.3. Comparison to Theory. The changes in dynamic properties that arise when a material is subject to stress have been the subject of much research. As discussed above, the dynamics in our systems are not constant for a given applied stress; while we do observe a fairly good correlation with the instantaneous strain rate in each system, the scatter in the data in Figures 9 and 10 implies that other variables, such as the applied stress or the heterogeneity of the potential energy landscape, likely have an interplay with the instantaneous strain rate and affect the dynamics. Here, we investigate how our results relate to models capable of describing stress-induced dynamics. Seventy years ago, Eyring proposed a phenomenological model to explain changes in viscosity in a material under stress.[21] In this model, the activation energy for a particle to hop "forward" (in the direction of applied stress) is linearly decreased with stress according to

$$k_f = \exp\left(-\frac{E_A - \sigma V}{k_B T}\right) \quad (4)$$

where k_f is the forward hopping rate, E_A is the activation energy, and V is an empirically defined activation volume. Similarly, the backward hopping rate is reduced according to

$$k_b = \exp\left(-\frac{E_A + \sigma V}{k_B T}\right) \quad (5)$$

and the relaxation time, τ, is then

$$1/\tau \propto \frac{e^{-E/k_B T}}{\sigma} \sinh\left(\frac{\sigma V}{k_B T}\right) \quad (6)$$

Equation 6 was originally derived for the viscosity, and here, we have assumed that $\tau \propto \eta$. Strain rate does not enter into the model of Eyring, although $k_f - k_b$ is often interpreted as the net current over the barrier. Figure 14 shows τ averaged over

the five $L_0 = 17.7$ configurations during each time window. Also shown in the figure 14 are the estimates of the τ when averaged over both configurations and time windows. We can fit these points to eq 6, and the results of this fitting procedure are shown in Figure 14; we find that eq 6 provides a reasonable description of our data and our best-fit values are $E_A = 6.28$ and $V = 2.71$. This value of E_A is approximately a factor of 3 larger than the activation energy obtained for this system at a very high temperature,[25] and the empirical volume V corresponds to roughly five monomer volumes. Additionally, we have shown above that our deformations increase the inherent structure energy, which would presumably also decrease E_A, and this effect is not taken into account in eq 6. This picture is also consistent with the ideas of the soft glass rheology (SGR) model,[38] although the SGR model considers strain as the relevant variable to decrease the energy barrier for plastic rearrangements. We point out that when we performed our fits in eqs 4 and 5 we replaced σ with $|\sigma|$, since the predictions of Eyring make no mention of the sign of the applied stress. There are, however, some differences between our results and the predictions of eq 6 that we wish to emphasize. First, according to eq 6, the reduction of τ should not depend on the direction of applied stress. Our results indicate that, for a given magnitude of applied stress, the dynamics in tension will be more enhanced than those in compression. Second, the derivation of eq 6 assumes that the dynamics are enhanced only in the direction of applied stress. This is qualitatively inconsistent with our results shown in Figure 11, where we show that the dynamics are uniformly enhanced in the directions perpendicular to the applied stress. Finally, for $\sigma V \gg k_B T$, $\log(\tau)$ should decrease linearly with σ. For our highest values of σ, eq 6 is clearly into this regime while our $\log(\tau)$ vs σ data still exhibits curvature, although better statistics are required to make a definitive statement.

Recently Chen and Schweizer have proposed a simple molecular-level theory at the level of forces for activated segmental barrier hopping[39,40] under stress in polymer glasses.[22] In this theory, external deformation results in a mechanical work type of contribution to a nonequilibrium free energy, which isotropically enhances the alpha relaxation time. Acceleration of the segmental relaxation time was predicted to be nearly exponential in stress with corrections that weaken its dependence relative to the Eyring result. Specific calculations of the relaxation time were performed for poly(methyl methacrylate) (PMMA). For a range of temperatures equal to and less than T_g, a nearly universal scaling behavior was predicted for the reduction of the relaxation time with stress. Over the first 2 orders of magnitude of alpha time decrease, the numerical results can be described very well by[22]

$$\text{Log}_{10}\frac{\tau(\tilde{\sigma})}{\tau(0)} = -0.17\tilde{\sigma}^{0.81}, \tag{7}$$

where $\tilde{\sigma} \equiv \sigma b^3/k_B T$ and b is the polymer statistical segment length. Equation 7 is consistent with the magnitude of the stress-induced acceleration of relaxation recently measured experimentally for PMMA.[4]

It is of interest to compare this theoretical result with our simulations. This requires a conversion of stress to units of $k_B T/\sigma_A^3$. Using the simulation value of $k_B T_g/\varepsilon_A = 0.37$, the PMMA parameters $b = \sigma_A \sim 1$ nm and $T_g = 378$ K,[22] one obtains

$$\text{Log}_{10}\frac{\tau(\sigma)}{\tau(0)} = -1.47\sigma^{0.81}. \tag{8}$$

Results based on this formula are plotted in Figure 14. Given the absence of adjustable parameters, the theoretical prediction is in good agreement with simulation. One apparent difference is the downward curvature of the simulation results, which is
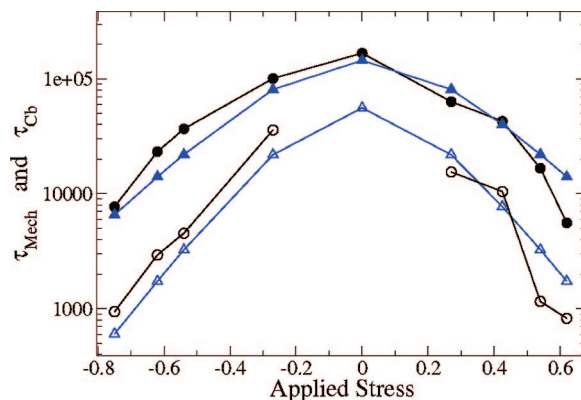

Figure 15. Relaxation times obtained from $C_b(t)$ averaged over both configurations and time windows at each stress (●) and their fit to eq 6 (▲). Also shown are τ_{Mech} (○) and the fit of those points to eq 6 (△).

not captured by eq 8. This could be due to several complications, in addition to the practical issue of simulation data scatter. First, the theory is for the slow α-relaxation, while the simulation results presented here extract a time scale from the late β and early α decay of the bond autocorrelation function. Hence, the question of possible interference between the fast and slow relaxation processes arises. More importantly, the theory was not integrated with a constitutive equation to describe creep. Additionally, the theory also ignored anisotropic chain conformations and stress-induced modification of the structure factor, the latter of which is the critical input to the dynamical theory. The simulation results presented here find that stress results in structural disordering ("rejuvenation") (see the discussion of Figure 3 above). In the context of the theory, this will reduce the confining dynamical constraints and accelerate even further the segmental relaxation process.[22] This represents a plausible physical mechanism for generating a downward curvature in the log(τ) versus stress plot of Figure 14. The theoretical roadblock is the lack of a predictive theory for how stress modifies $S(q)$, although this problem is under study.[41] Given the relatively good agreement of both theoretical predictions with our simulation results, it would be of interest in a future study to perform creep deformations at larger values of applied stress, where we expect the differences between the two theoretical predictions to become more pronounced.

3.4. Mechanical Relaxation Time. We can calculate a mechanical relaxation time for our systems by considering the simple Maxwell mechanical model for the creep compliance,

$$J(t) = 1/E + t/\eta. \tag{9}$$

Here, E is an effective elastic constant (the stiffness of the spring in the Maxwell model), and η is the viscosity of the dashpot. To a first approximation, we can determine E by assuming that the initial strain response of our systems (i.e., the first measurement of the strain after applying the stress) is a purely elastic response. After averaging over all configurations and values of applied stress, we find that $E = 32.2$. Next, we can obtain η from eq 9 from the limiting slope of the plot of strain versus time for each stress shown in Figure 1b. Note that in order to obtain η we perform our linear fits to the data sampled from the final 2000 time points. Finally, we can obtain an effective mechanical relaxation time by taking $\tau_{\text{Mech}} = \eta/E$; results for τ_{Mech} at each applied stress are shown in Figure 15. Also shown in Figure 15 are fits of τ_{Mech} to eq 6, which again provides a reasonable description of our data. For the fits to τ_{Mech}, we find that $E_A = 6.77$ and $V = 3.55$; while this estimate of E_A is comparable to the value of E_A obtained from fitting τ from the bond autocorrelation function, this estimate of V is

larger and corresponds to nearly seven monomer volumes. It is interesting to note that the relative changes in the mechanical relaxation times are approximately the same as those measured from $C_b(t)$.

4. Conclusions

In this study, we have extended our previous work,[17] which showed that changes in molecular mobility are related to strain rate and demonstrated that changes in the free volume could not provide an explanation for that effect. Here, we have explored the nonlinear creep response of our model polymer in more detail. We have found that the overall structure, as measured by the structure factor, $S(q)$, changes after deformation; additionally, the dimensions of the polymer chains are significantly deformed. By studying the dynamics in our material, we have found that the dynamics are significantly enhanced by the applied stress and we have also observed that the most pronounced enhancements occur during times of high strain rate. The dynamics are apparently enhanced isotropically and uniformly over the two length scales investigated here. We propose that a potential energy landscape picture can offer an explanation of the observed enhanced dynamics. During the periods of high strain rate, the system exhibits faster dynamics and higher inherent structure potential energies during both compression and tension. Our results were discussed in terms of the Eyring model and a more recently proposed model of segmental barrier hopping in polymer glasses under stress.[22]

References and Notes

(1) Loo, L.; Cohen, R.; Gleason, K. *Science* **2000**, *288*, 116.
(2) Zhou, Q. Y.; Argon, A. S.; Cohen, R. E. *Polymer* **2001**, *42*, 613.
(3) Nealey, P. F.; Cohen, R. E.; Argon, A. S. *Polymer* **1995**, *36*, 3687.
(4) Lee, H.-N.; Pang, K.; Swallen, S. F.; Ediger, M. D., *J. Chem. Phys.* **2008**, *128*, 134902.
(5) Isner, B. A.; Lacks, D. J. *Phys. Rev. Lett.* **2006**, *96*, 025506.
(6) Lacks, D. J. *Phys. Rev. Lett.* **2001**, *87*, 225502.
(7) Frey, M. M.; Lacks, D. J. *J. Chem. Phys.* **2000**, *112*, 2909.
(8) Berthier, L.; Barrat, J.-L. *J. Chem. Phys.* **2002**, *116*, 6228.
(9) Varnik, F. *J. Chem. Phys.* **2006**, *125*, 164514.
(10) Nandagopal, M.; Utz, M. *J. Chem. Phys.* **2003**, *118*, 8373.
(11) Utz, M.; Peng, Q.; Nandagopal, M. *J. Poly. Sci., B: Poly. Phys.* **2004**, *42*, 2057.
(12) Capaldi, F. M.; Boyce, M. C.; Rutledge, G. C. *Phys. Rev. Lett.* **2002**, *89*, 175505.
(13) Capaldi, F. M.; Boyce, M. C.; Rutledge, G. C. *Polymer* **2004**, *45*, 1391.
(14) Lyulin, A. V.; Balabaev, N. K.; Mazo, M. A.; Michels, M. A. J. *Macromolecules* **2004**, *37*, 8785.
(15) Lyulin, A. V.; Vorselaars, B.; Mazo, M. A.; Balabaev, N. K.; Michels, M. A. J. *Europhys. Lett.* **2005**, *71*, 618.
(16) Warren, M.; Rottler, J. *Phys. Rev. E* **2007**, *76*, 031802.
(17) Riggleman, R. A.; Lee, H.-N.; Ediger, M. D.; de Pablo, J. J. *Phys. Rev. Lett.* **2007**, *99*, 215501.
(18) Léonforte, F.; Tanguy, A.; Wittmer, J.; Barrat, J.-L. *Phys. Rev. Lett.* **2006**, *97*, 055501.
(19) Léonforte, F.; Boissiere, R.; Tanguy, A.; Wittmer, J. P.; Barrat, J.-L. *Phys. Rev. B* **2005**, *72*, 224206.
(20) Léonforte, F.; Tanguy, A.; Wittmer, J. P.; Barrat, J.-L. *Phys. Rev. B* **2004**, *70*, 014203.
(21) Eyring, H. *J. Chem. Phys.* **1936**, *4*, 283.
(22) Chen, K.; Schweizer, K. S. *Euro. Phys. Lett.* **2007**, *79*, 26006.
(23) Jain, T. S.; de Pablo, J. J. *J. Chem. Phys.* **2005**, *122*, 174515.
(24) Riggleman, R. A.; Yoshimoto, K.; Douglas, J. F.; de Pablo, J. J. *Phys. Rev. Lett.* **2006**, *97*, 045502.
(25) Riggleman, R. A.; Douglas, J. F.; de Pablo, J. J. *J. Chem. Phys.* **2007**, *126*, 234903.
(26) Riggleman, R. A.; Douglas, J. F.; de Pablo, J. J. *Phys. Rev. E* **2007**, *76*, 011504.
(27) Jain, T.; de Pablo, J. *Phys. Rev. Lett.* **2004**, *92*, 155505.
(28) Parrinello, M.; Rahman, A. *J. Chem. Phys.* **1982**, *76*, 2662.
(29) Berendsen, H. J. C.; van der Spoel, D.; van Drunen, R. *Comput. Phys. Commun.* **1995**, *91*, 45–56.
(30) Lindahl, E.; Hess, B.; van der Spoel, D. *J. Mol. Model.* **2001**, *7*, 306–317.
(31) Papakonstantopoulos, G. J.; Doxastakis, M.; Nealey, P. F.; Barrat, J.-L.; de Pablo, J. J. *Phys. Rev. E* **2007**, *75*, 031803.
(32) Struik, L. C. E. *Physical Aging in Amorphous Polymers and Other Materials*; Elsevier: New York, NY, 1978.
(33) Bennemann, C.; Paul, W.; Baschnagel, J.; Binder, K. *J. Phys.: Condens. Matter* **1999**, *11*, 2179.
(34) Stillinger, F. H.; Weber, T. A. *Phys. Rev. A* **1983**, *28*, 2408.
(35) Goldstein, M. *J. Chem. Phys.* **1969**, *51*, 3728–3739.
(36) Sastry, S.; Debenedetti, P.; Stillinger, F. *Nature* **1998**, *393*, 554–557.
(37) Utz, M.; Debenedetti, P. G.; Stillinger, F. H. *Phys. Rev. Lett.* **2000**, *84*, 1471.
(38) Sollich, P.; Lequeux, F.; Hébraud, P.; Cates, M. E. *Phys. Rev. Lett.* **1997**, *78*, 2020.
(39) Schweizer, K. S.; Saltzman, E. J. *J. Chem. Phys.* **2004**, *121*, 1984.
(40) Saltzman, E. J.; Schweizer, K. S. *J. Chem. Phys.* **2004**, *121*, 2001.
(41) Chen, K.; Schweizer, K. S. Unpublished.